35th Annual International Conference of the IEEE EMBS
Osaka, Japan, 3 - 7 July, 2013

Anatomical Variability Predicts Individual Differences in Transcranial Electric Stimulation Motor Threshold

Won Hee Lee, *Student Member, IEEE*, Sarah H. Lisanby, Andrew F. Laine, *Fellow, IEEE*, and Angel V. Peterchev, *Member, IEEE*

***Abstract*—We have proposed that the current amplitude in electroconvulsive therapy (ECT) be lowered to produce stimulation closer to the neural activation threshold and individualized to account for anatomical variability across patients. A novel approach to individualize the ECT current amplitude could be via motor threshold (MT) determination with transcranial electric stimulation (TES) applied through the ECT electrodes instead of the fixed high current approach. This study derives an estimate of the electric field (E-field) neural activation threshold and tests whether individual differences in TES MT are explained by anatomical variability measurements and simulations in individual head models. The E-field distribution induced by a right unilateral (RUL) ECT electrode configuration was computed in subject-specific finite element head models of four nonhuman primates (NHPs) for whom MT was measured. By combining the measured MTs and the computed E-field maps, the neural activation threshold is estimated to be 0.45 ± 0.07 V/cm for 0.2 ms stimulus pulse width. The individual MT was correlated with the electrode-to-cortex distance under the superior electrode (R^2=.96, p=.022) as well as with the simulated electrode-current/induced-E-field ratio (R^2=.95, p=.026), indicating that both anatomical measurements and computational models could predict the individual current requirements for transcranial stimulation. These findings could be used with realistic human head models and in clinical studies to explore novel ECT dosing paradigms, and as a new noninvasive means to determine individual dosage requirement with ECT.**

I. Introduction

ELECTROCONVULSIVE therapy (ECT) is a highly effective treatment for psychiatric disorders such as depression, but some patients experience cognitive side effects [1]. We have proposed that lowering and individualizing the stimulus current amplitude could reduce the side effects of ECT [2]. Lowering of the ECT stimulus current is supported by observations that conventional current amplitudes result in very broad brain stimulation with electric field (E-field) strength that exceeds the neural activation threshold by several fold [3]. Individualizing of the stimulus current is supported by the significant variability in the E-field characteristics that is estimated to result from anatomical variability but has yet to be attempted [4], [5]. These observations are based, in part, on simplified spherical head models and neural activation thresholds estimated from studies done under different conditions than ECT procedures [4] or on electrode configurations that are substantially different from those used in ECT [5]. In this paper we aim to estimate the neural activation threshold in conditions matching ECT procedures and to evaluate how well a simple motor threshold (MT) titration procedure could be used for individualizing the current amplitude by accounting for individual anatomical variability in a nonhuman primate (NHP) model of ECT. These data could then be used with realistic human models [6] and in clinical studies to explore novel ECT dosing paradigms, and as a novel noninvasive means to determine individual dosage requirement for ECT.

MT is the threshold pulse amplitude required to elicit a muscle twitch. It is commonly used in transcranial magnetic stimulation (TMS) to individualize the amplitude of stimulus trains in repetitive TMS paradigms and to reduce the risk of inadvertent seizure [7], since it captures the effect of anatomical variability on the E-field induced in the brain as well as individual variation in neural excitability. Similarly, MT can be determined with transcranial electric stimulation (TES) delivered through the electrodes used for ECT [8].

If the MT data is coupled with a model of the E-field induced in the brain, the threshold E-field strength for neural activation can be estimated [9]. The E-field strength induced by TES in the brain can be simulated by computational models using the finite element method (FEM) [3]-[6]. A realistic, individual head model captures the effects of the subject's anatomy. The current corresponding to individual MT can be injected into the model, resulting in E-field strength in the motor cortex controlling the target muscle that corresponds to the neural activation threshold.

This study is an extension of our previous single-subject study [9]. We test the hypothesis that individual differences in TES MT are explained by anatomical variables and can be predicted by a subject-specific simulation model. We create realistic finite element models of four NHP heads to simulate the spatial distribution of the E-field strength generated by a right unilateral (RUL) ECT electrode configuration. We also use measured TES MT data for these subjects to estimate the E-field threshold for neural activation in the motor cortex.

This work was supported by NIH grant R01MH091083.

W. H. Lee is with the Department of Biomedical Engineering, Columbia University, New York, NY 10027 and with the Department of Psychiatry and Behavioral Sciences, Duke University, Durham, NC 27710, USA (e-mail: wl2324@columbia.edu).

S. H. Lisanby is with Department of Psychiatry and Behavioral Sciences, and Department of Psychology & Neuroscience, Duke University, Durham, NC 27710, USA (e-mail: sarah.lisanby@duke.edu).

A. F. Laine is with the Department of Biomedical Engineering, Columbia University, New York, NY 10027, USA (e-mail: laine@columbia.edu).

A. V. Peterchev is with Departments of Psychiatry and Behavioral Sciences, Biomedical Engineering, and Electrical and Computer Engineering, Duke University, Durham, NC 27710, USA (phone: 919-684-0383; fax: 919-681-9962; e-mail: angel.peterchev@duke.edu).

978-1-4577-0216-7/13/$26.00 ©2013 IEEE

II. Methods

A. Structural and Diffusion Tensor MRI Acquisition

All studies were approved by the Institutional Animal Care and Use Committees of New York State Psychiatric Institute, Columbia University, and Duke University. T1-weighted magnetic resonance imaging (MRI) and diffusion-weighted imaging (DWI) data sets of four healthy male rhesus macaques (*Macaca mulatta*) (age=12–18 years; weight=8.4–10.7 kg) were acquired on a Siemens 3T Trio scanner using an 8-channel knee coil. The T1-weighted images were acquired with a 3D MPRAGE sequence (TR=2300 ms; TE=4.4 ms; TI=1100 ms; 256 coronal slices; 0.7×0.7×0.7 mm^3 voxel; FA=8º; 2 averages). The DWI data were acquired by employing a single-shot spin-echo EPI sequence (TR=13000 ms; TE=81 ms; 128×128 matrix; 1.4×1.4×1.4 mm^3 voxel; ; 6 averages). The diffusion sensitizing gradients with a b-value of 1000 s/mm^2 were applied in 12 non-collinear directions. The DWI data were corrected for the distortions due to eddy currents and possible motion artifacts. Diffusion tensors were determined and then coregistered onto the structural images using FSL [10].

B. TES Finite Element Head Model Generation

The generation of a NHP head model started with preprocessing of the structural T1-weighted MRI images. As a first step, we extracted the monkey head regions from background noise and artifacts using a morphological processing technique including thresholding, opening, and closing of the head binary masks [6]. The head MRI images were upsampled (0.5×0.5×0.5 mm^3 voxel) and were spatially oriented along manually-defined anatomical landmarks, corresponding to anterior commissure, posterior commissure, and fiducials for inter-hemispheral midline. The MRI image intensities were corrected for bias field inhomogeneity [11]. We then applied content-preserving anisotropic diffusion filtering to remove the image noise while preserving content details and enhancing tissue boundaries [9]. Finally, non-brain regions were removed using the skull-stripping algorithm in FSL [10]. As a second step, we implemented an automatic algorithm that adopts the "unified segmentation" approach in SPM8 [12]. The de-skulled MRI images were automatically segmented into tissue probability images corresponding to gray matter, white matter, and cerebrospinal fluid (CSF) based on the macaque tissue priors [13]. The non-brain regions were manually segmented into 11 different tissue compartments, including skin, muscle, skull spongiosa, skull compacta, vertebrae, spinal cord, lens, eyeball, sclera, optic nerve, and sinus, using an in-house segmentation algorithm and the ITK-SNAP software [14]. As a third step, we modeled the stimulation round electrodes (2.5 cm diameter) for the RUL electrode placement and properly positioned to the NHP head models (see Fig. 1) modeling the RUL configuration in clinical ECT [9]. As a last step, we applied adaptive finite element meshing technique to the individual NHP head models incorporating the stimulation electrodes. The individual-specific TES finite element models of the four heads were created by means of the restricted Delaunay tessellation algorithm [15].

TABLE I
Tissue Electrical Conductivities (S/m)

Tissue	Conductivity	Tissue	Conductivity
Skin	0.43	Spinal cord	0.15
Muscle	0.32	Vertebrae	0.012
Skull compacta	0.0063	Lens	0.32
Skull spongiosa	0.04	Eyeball	0.5
Cerebrospinal fluid	1.79	Sclera	0.5
Gray matter	0.33	Optic nerve	0.14
White matter (iso.)	0.14	Sinus	0

C. Electric Field Computation

We created volume conductor head models by assigning anisotropic electrical conductivities to the white matter compartment, and isotropic conductivities to all other tissue regions. The isotropic electrical conductivity values are listed in Table I [6]. The conductivity tensors in the white matter were computed using the volume normalized approach [16, 17], where the eigenvalues of the conductivity tensor match the eigenvalues of the diffusion tensor, and the conductivity tensor is scaled so that its volume equals that of an isotropic conductivity tensor with conductivity given in Table I (volume constraint).

To determine the E-field distribution in each head model, the Laplace equation was solved using the preconditioned conjugate solver in ANSYS (ANSYS Inc., Canonsburg, PA, USA) [6].

D. In Vivo Motor Threshold Titration

The MT was defined as the lowest stimulus amplitude of a single pulse required to elicit a motor response [8]. We determined the individual MTs by adjusting the amplitude of single stimulus pulses (pulse width = 0.2 ms) delivered through the RUL ECT electrodes in the four anesthetized NHP subjects. The MTs were determined by measuring the motor evoked potentials of the first dorsal interosseous (FDI) muscle in the left hand, since the RUL electrode configuration predominantly stimulates the right hemisphere [9]. We determined the MT as the minimum stimulus pulse amplitude needed to achieve a 50 μV peak-to-peak motor evoked potential for at least five out of ten trials. The MT titration was repeated three times for each subject and each current direction, and the six thresholds were averaged per subject.

E. Neural Activation Threshold Estimate

Individual neural activation threshold was estimated as the median E-field strength in the FDI representation of the motor cortex at the current strength corresponding to the individual MT [9]. The individual cortical FDI representations, shown in Fig. 1, were delineated manually based on a stereotaxic atlas [18].

F. Anatomical Predictors of Motor Threshold

Since the tissue thickness between the electrode and cortex is a critical determinant of the amount of stimulus current reaching the cortex, we examined the relation between the

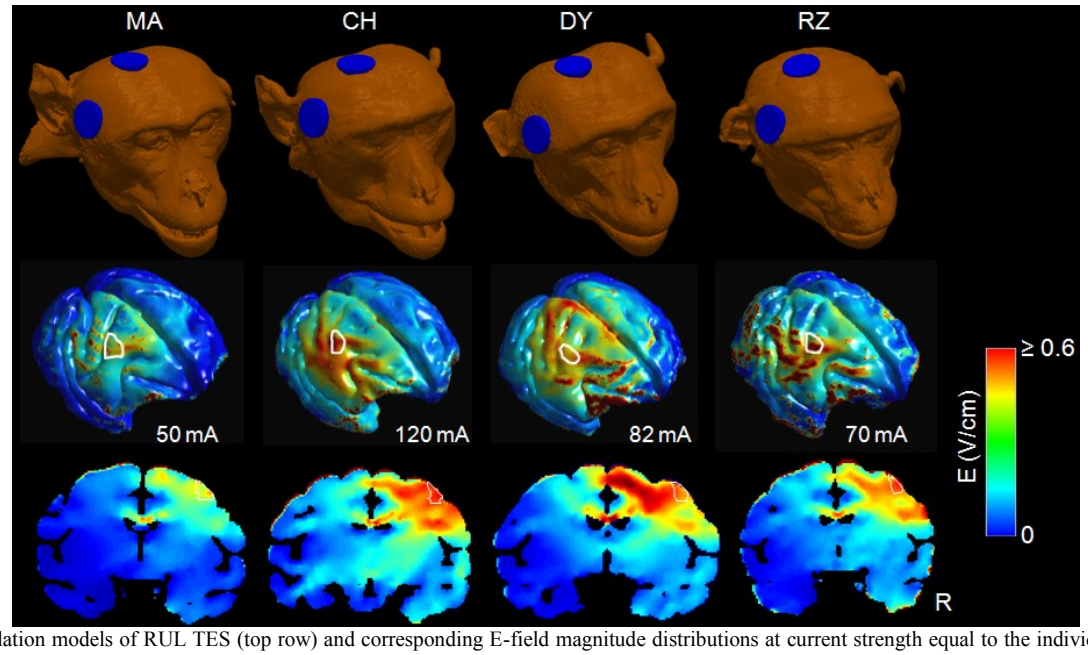

Fig. 1. Simulation models of RUL TES (top row) and corresponding E-field magnitude distributions at current strength equal to the individually titrated motor threshold (MT) of first dorsal interosseous (FDI) (shown below second row) on the cortical surface (second row) and in a coronal slice (bottom row) for four NHP subjects (left to right columns, respectively). Region-of-interest outlines in white show FDI motor area. R: right.

measured MT and the electrode-to-cortex thickness under the electrode centers and at vertex.

Based on the FEM model simulations, we also calculated the ratio of the electrode current to the median FDI E-field strength, $I_{\text{electrode}}/E_{\text{FDI}}$, for each subject. This ratio is expected to be correlated with the individual MTs since it characterizes the amount of current that has to be applied so that the FDI region in motor cortex reaches a fixed neural activation threshold. The underlying assumption here is that the E-field neural activation threshold is comparable among the subjects. The extent to which this is the case will be evaluated as described in section II-E.

III. Results

The mean MT is 80.3 mA (range=50–120 mA, coefficient of variation=0.37). Fig. 1 shows the simulated RUL TES electrode montages for the four NHP models (top row) and the spatial E-field magnitude distributions at the individual MT current on the cortical surface (second row) and in a representative coronal slice (bottom row).

Fig. 2 shows estimates of the individual E-field neural activation threshold for each subject. Subject CH has the highest E-field threshold (0.52 V/cm), whereas subject MA has the lowest E-field threshold (0.35 V/cm). The mean E-field threshold is 0.45 V/cm (range=0.35–0.52 V/cm, standard deviation=0.07).

Fig. 3 (a) shows the correlation between the measured MT and the electrode-to-cortex distance in the region underlying the superior electrode that borders the vertex (R^2=.96, p=.022). We also found a strong correlation between MT and the distance between the scalp surface at vertex and the cortical surface (R^2=.98, p=.0007). However, there was no significant correlation between MT and the electrode-to-cortex distance for the right frontotemporal electrode (R^2=.27, p=.476), which is remote from primary motor cortex.

Fig. 3 (b) shows the correlation between the $I_{\text{electrode}}/E_{\text{FDI}}$ ratio computed from the individual FEM models and the measured MT. This correlation characterizes the ability of the computational model to predict the individual variability in MT. The correlation is strong (R^2=.95, p=.026), even for this small sample of subjects.

IV. Discussion and Conclusions

Based on the individual MTs of the left FDI muscle and the E-field models, the neural activation threshold was estimated to be 0.45 ± 0.07 V/cm for the 0.2 ms rectangular pulses. The variability in the neural activation threshold estimate could be due to individual differences in neural excitability or brain anatomy in the FDI motor area, and/or to modeling errors. Furthermore, we cannot exclude that neural stimulation may have occurred along the corticospinal tract away from the cortical representation of FDI. Nevertheless, the strong correlation between the MT and the E-field in the cortical FDI

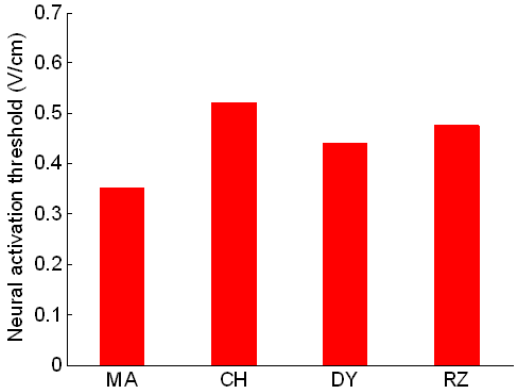

Fig. 2. Estimated E-field neural activation threshold in the motor cortex representation of FDI for stimulus pulse width of 0.2 ms in four NHP subjects.

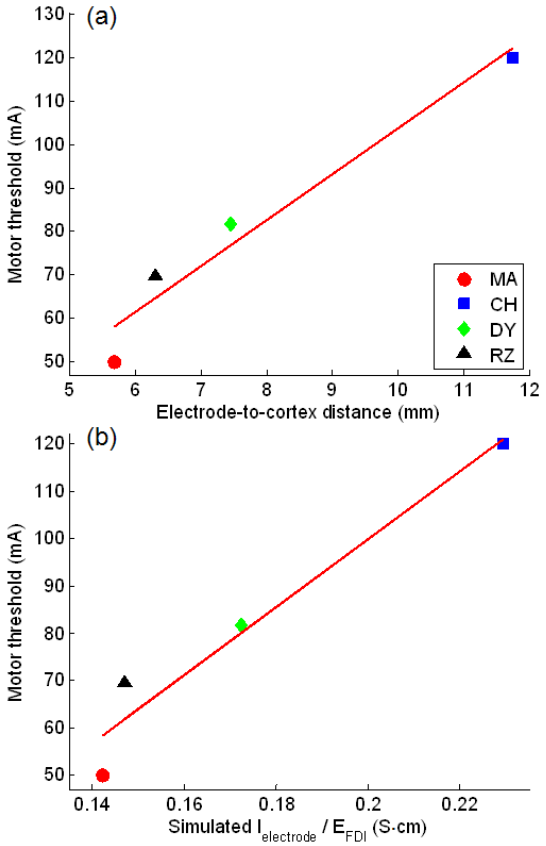

Fig. 3. Correlation between the measured MT and (a) the electrode-to-cortex distance under the superior stimulation electrode (R^2=.96, p=.022), or (b) the $I_{electrode}/E_{FDI}$ ratio computed from the individual FEM models (R^2=.95, p=.026).

control area as well as the superior-electrode-to-cortex and vertex-to-cortex distances does support cortical origin of the motor evoked potentials. Further, the variation in the neural activation thresholds (16%) was smaller than the variation in the MTs (37%) indicating that the FEM models indeed account for interindividual differences in anatomy.

The lack of correlation between MT and the distance between the frontotemporal electrode and cortex could potentially be explained by the significantly larger electrode-to-cortex distance at that location compared to the vicinity of vertex. This may be due to the large lateral muscles in the NHP head, which result in less penetration of the electrode current into the intracranial space at lateral compared to superior locations. This may also relate to the longer distance between the lateral electrode and the FDI cortical motor area. The small number of subjects in the study could also affect the correlation analyses.

Finally, the strong correlation between MT and the simulated $I_{electrode}/E_{FDI}$ ratio suggests that FEM models could predict variations in the individual current required for neural stimulation in TMS, ECT and in other transcranial stimulation applications.

V. Acknowledgement

The authors thank Christopher Sikes-Keilp, Mohamed Aly, Brian Chan, Niko Reyes, Moacyr A. Rosa, and Nagy Youssef for assisting in the NHP procedures and data entry. We would like to thank Drs. Richard Weiner and Andrew Krystal from the Department of Psychiatry and Behavioral Sciences at Duke University for their helpful comments and suggestions.

VI. References

[1] R. Abrams, *Electroconvulsive therapy*, 4th Ed. New York: Oxford Unversity Press, 2002.

[2] A. V. Peterchev, M. A. Rosa, Z. D. Deng, J. Prudic, and S. H. Lisanby, "Electroconvulsive therapy stimulus parameters: rethinking dosage," *J. ECT,* vol. 26, pp. 159-174, 2010.

[3] Z. D. Deng, S. H. Lisanby, and A. V. Peterchev, "Electric field strength and focality in electroconvulsive therapy and magnetic seizure therapy: a finite element simulation study," *J. Neural Eng.,* vol. 8, 2011.

[4] Z. D. Deng, S. H. Lisanby, and A. V. Peterchev, "Effect of anatomical variability on neural stimulation strength and focality in electroconvulsive therapy (ECT) and magnetic seizure therapy (MST)," *Conf. Proc. IEEE Eng. Med. Biol. Soc.,* vol. 2009, pp. 682-688, 2009.

[5] D. Edwards, M. Cortes, A. Datta, P. Minhas, E. M. Wassermann, and M. Bikson, "Physiological and moddeling evidence for focal transcranial electrical brain stimulation in humans: a basis for high-definition tDCS," *NeuroImage,* vol. 74, pp. 266-275, 2013.

[6] W. H. Lee, Z. D. Deng, T. S. Kim, A. F. Laine, S. H. Lisanby, and A. V. Peterchev, "Regional electric field induced by electroconvulsive therapy in a realistic finite element head model: influence of white matter anisotropic conductivity," *NeuroImage,* vol. 59, pp. 2110-2123, 2012.

[7] S. Rossi, M. Hallett, P. M. Rossini, and A. Pascual-Leone; Safety of TMS Consensus Group, "Safey, ethical considerations, and application guidelines for the use of transcranial magnetic stimulation in clinical practice and research," *Clin. Neurophysiol.,* vol. 120, pp. 2008-2039, 2009.

[8] A. V. Peterchev, B. Chan, and S. H. Lisanby, "Pulse amplitude adjustment: a novel means of individualizing and predicting dosage requirements for electroconvulsive therapy and magnetic seizure therapy," *J. ECT,* vol. 26, p. 154, 2010.

[9] W. H. Lee, S. H. Lisanby, A. F. Laine, and A. V. Peterchev, "Stimulaton strength and focality of electroconvulsive therapy with individualized current amplitude: a preclinical study," *Conf. Proc. IEEE Eng. Med. Biol. Soc., pp. 6430-6433, 2012.*

[10] S. M. Smith, M. Jenkinson, M. W. Woolrich, C. F. Beckmann, T. E. Behrens, H. Johansen-Berg, P. R. Bannister, M. De Luca, I. Drobnjak, D. E. Flitney, R. K. Niazy, J. Saunders, J. Vickers, Y. Zhang, N. De Stefano, J. M. Brady, and P. M. Matthews, "Advances in functional and structural MR image analysis and implementation as FSL," *NeuroImage,* vol. 23 Suppl 1, pp. S208-219, 2004.

[11] N. J. Tustison, B. B. Avants, P. A. Cook, Y. Zheng, A. Egan, P. A. Yushkevich, and J. C. Gee, "N4ITK: improved N3 bias correction," *IEEE Trans. Med. Imaging,* vol. 29, pp. 1310-1320, 2010.

[12] J. Ashburner and K. J. Friston, "Unified segmentation," *NeuroImage,* vol. 26, pp. 839-851, 2005.

[13] D. G. McLaren, K. J. Kosmatka, T. R. Oakes, C. D. Kroenke, S. G. Kohama, J. A. Matochik, D. K. Ingram, and S. C. Johnson, "A population-average MRI-based atlas collection of the rhesus macaque," *NeuroImage,* vol. 45, pp. 52-59, 2009.

[14] P. A. Yushkevich, J. Piven, H. C. Hazlett, R. G. Smith, S. Ho, J. C. Gee, and G. Gerig, "User-guided 3D active contour segmentation of anatomical structures: significantly improved efficiency and reliability," *NeuroImage,* vol. 31, pp. 1116-1128, 2006.

[15] J. P. Pons, E. Segonne, J. D. Boissonnat, L. Rineau, M. Yvinec, and R. Keriven, "High-quality consistent meshing of multi-label datasets," *Inf. Process. Med. Imaging,* vol. 20, pp. 198-210, 2007.

[16] D. S. Tuch, V. J. Wedeen, A. M. Dale, J. S. George, and J. W. Belliveau, "Conductivity tensor mapping of the human brain using diffusion tensor MRI," *Proc. Natl. Acad. Sci.,* vol. 98, pp. 11697-11701, 2001.

[17] H. Hallez, S. Staelens, and I. Lemahieu, "Dipole estimation errors due to not incorporating anisotropic conductivities in realistic head models for EEG source analysis," *Phys. Med. Biol.,* vol. 54, pp. 6079-6093, 2009.

[18] G. Paxinos, X. F. Huang, and A. W. Toga, *The rhesus monkey brain in stereotaxic coordinates*. San Diego: Academic Press, 1999.